**Supporting Information**

# Corner-opened cage-silsesquioxane as a directional template for tripodal poly(methyl methacrylate)

Ryota Tanaka,[a] Amato Igarashi,[a] Taihei Hayashi,[a] Hiroyasu Masunaga,[b] Hideaki Takagi,[c] Nobutaka Shimizu,[c] Noriyuki Igarashi,[c] Shinichi Sakurai,[d] Hiroaki Imoto*[a,e] and Kensuke Naka*[a,f]

a. Faculty of Molecular Chemistry and Engineering, Kyoto Institute of Technology, Goshokaido-cho, Matsugasaki, Sakyo-ku, Kyoto 606-8585, Japan. E-mail: himoto@kit.ac.jp (HI), kenaka@kit.ac.jp (KN).

b. Japan Synchrotron Radiation Research Institute (JASRI/SPring-8), Hyogo 679-5198, Japan.

c. Photon Factory, High Energy Research Organization, Oho, Tsukuba Ibaraki 305-0801, Japan

d. Department of Biobased Materials Science, Kyoto Institute of Technology, Goshokaido-cho, Matsugasaki, Sakyo-ku, Kyoto, 606-8585, Japan.

e. FOREST, JST, Honcho 4-1-8, Kawaguchi, Saitama 332-0012, Japan.

f. Materials Innovation Lab, Kyoto Institute of Technology, Goshokaido-cho, Matsugasaki, Sakyo-ku, Kyoto 606-8585, Japan.

**Contents:**

1. NMR spectra
2. MALDI-TOF MS spectra
3. SEC traces
4. SAXS analyses on the aggregation structures
5. More detailed discussion on the aggregated particles

## 1. NMR spectra

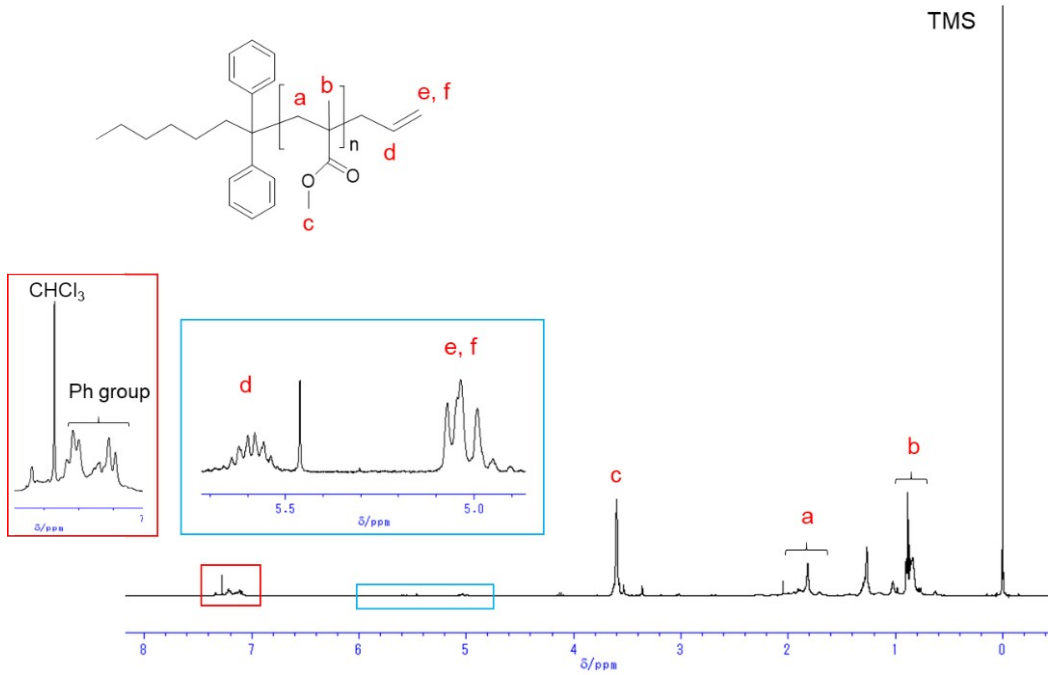


**Figure S1.** $^{1}$H-NMR spectrum (400 MHz) of **1a** in $CDCl_3$.

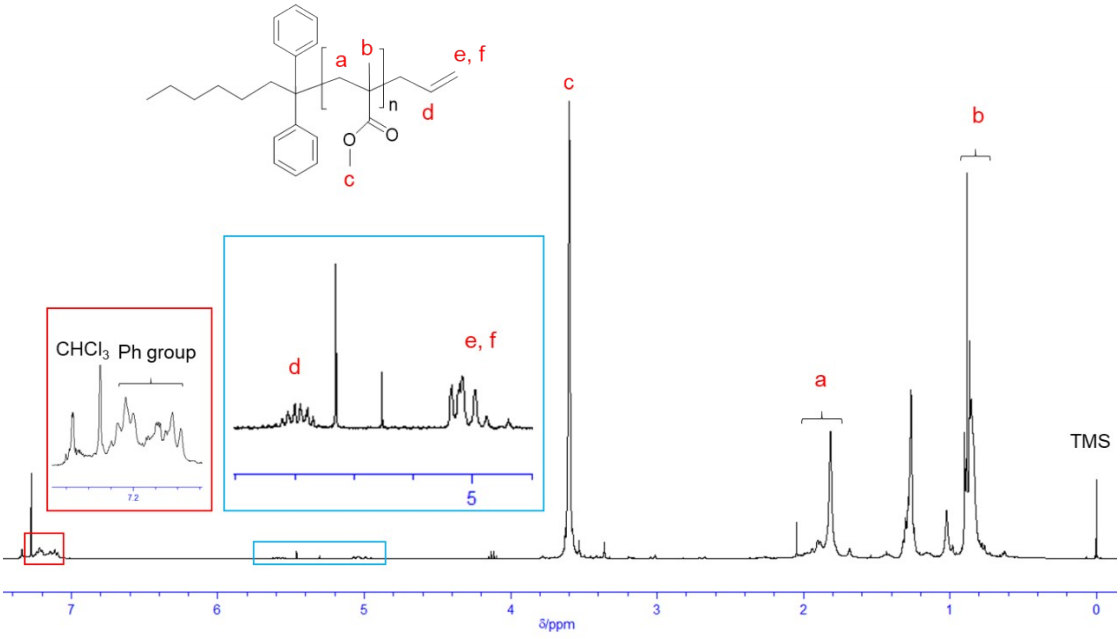


**Figure S2.** $^{1}$H-NMR spectrum (400 MHz) of **1b** in $CDCl_3$.

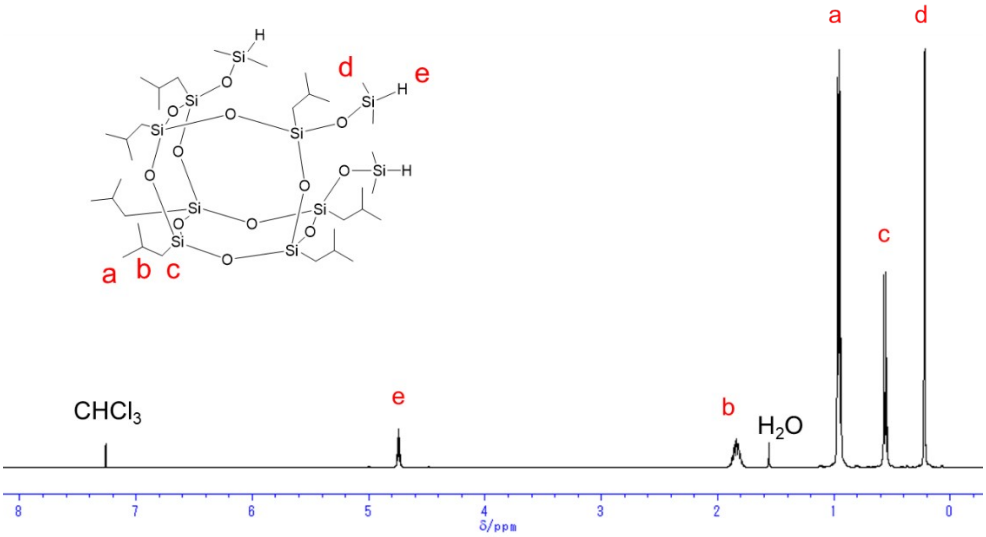


**Figure S3.** $^{1}$H-NMR spectrum (400 MHz) of **2a** in $CDCl_3$.

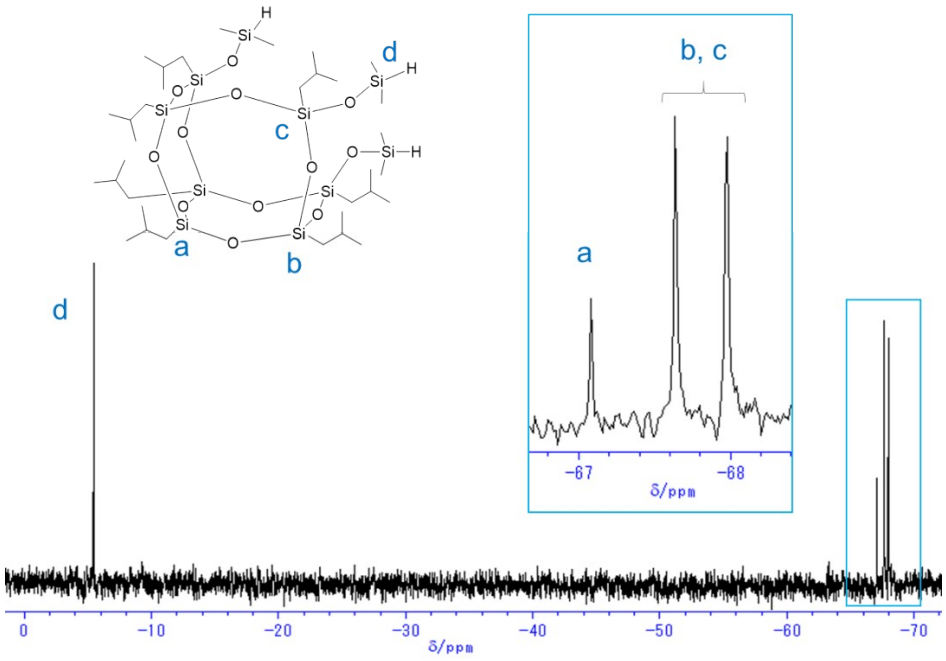


**Figure S4.** $^{29}$Si-NMR spectrum (80 MHz) of **2a** in $CDCl_3$.

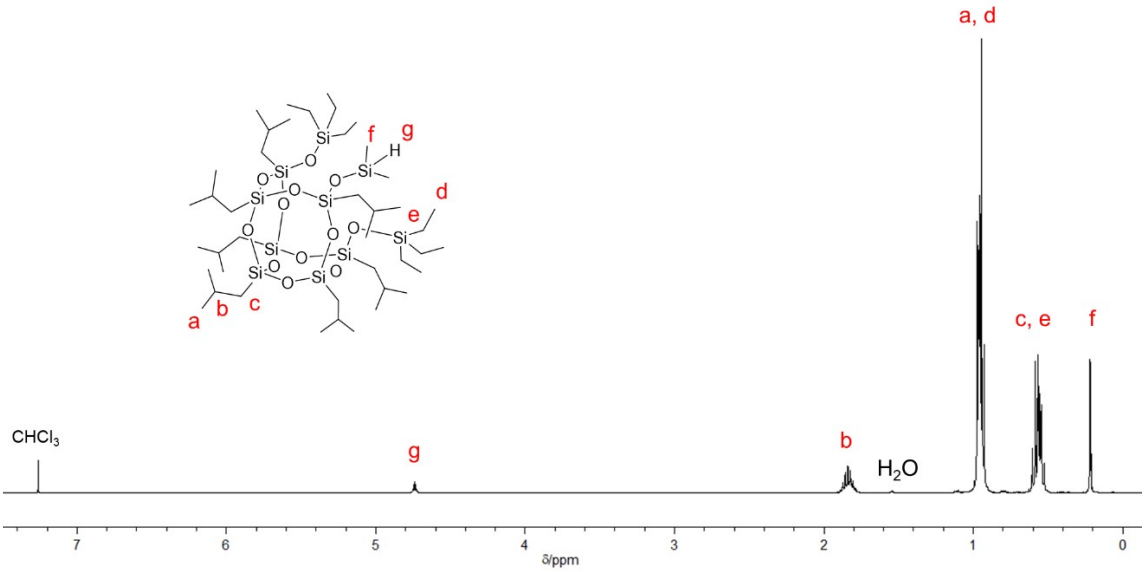


**Figure S5.** $^{1}$H-NMR spectrum (400 MHz) of **2b** in $CDCl_3$.

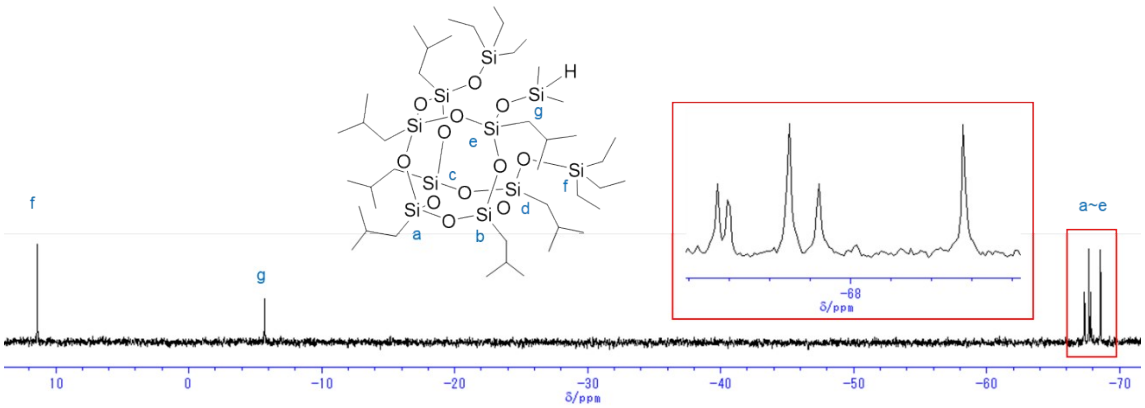


**Figure S6.** $^{29}$Si-NMR spectrum (80 MHz) of **2b** in $CDCl_3$.

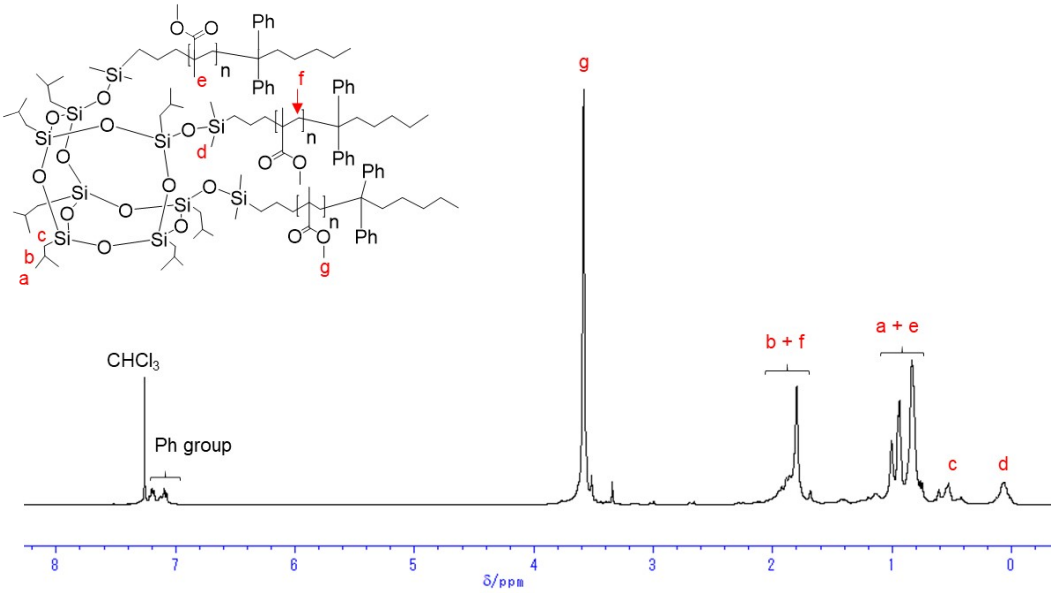


**Figure S7.** $^{1}$H-NMR spectrum (400 MHz) of **3a** in $CDCl_3$.

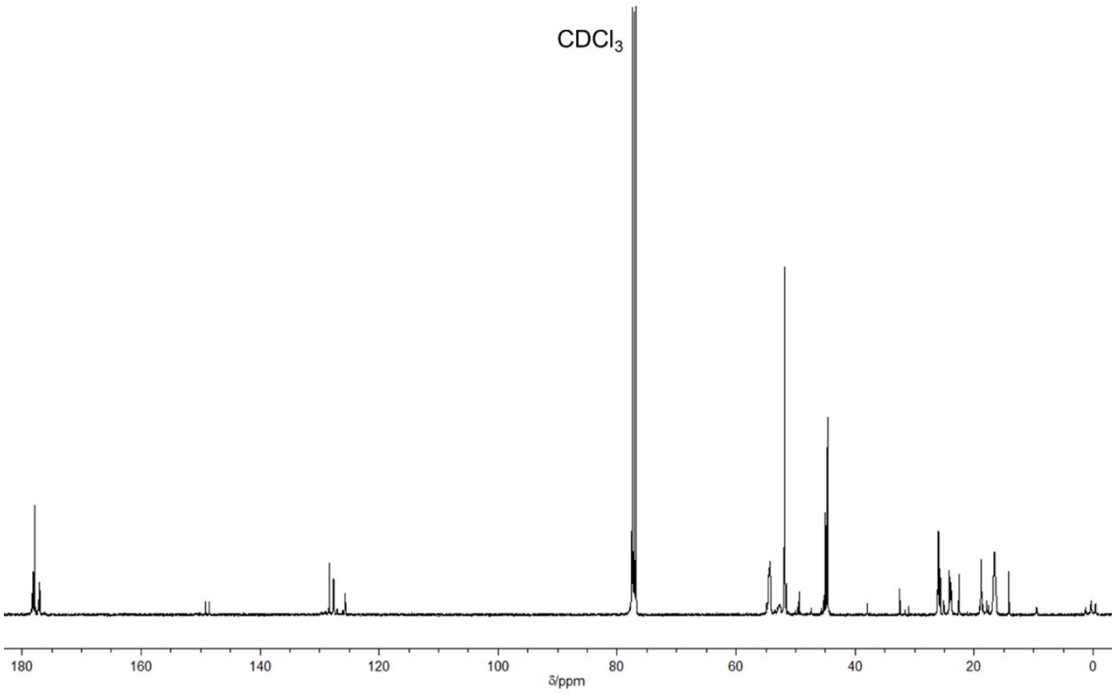


**Figure S8.** $^{13}$C-NMR spectrum (100 MHz) of **3a** in $CDCl_3$.

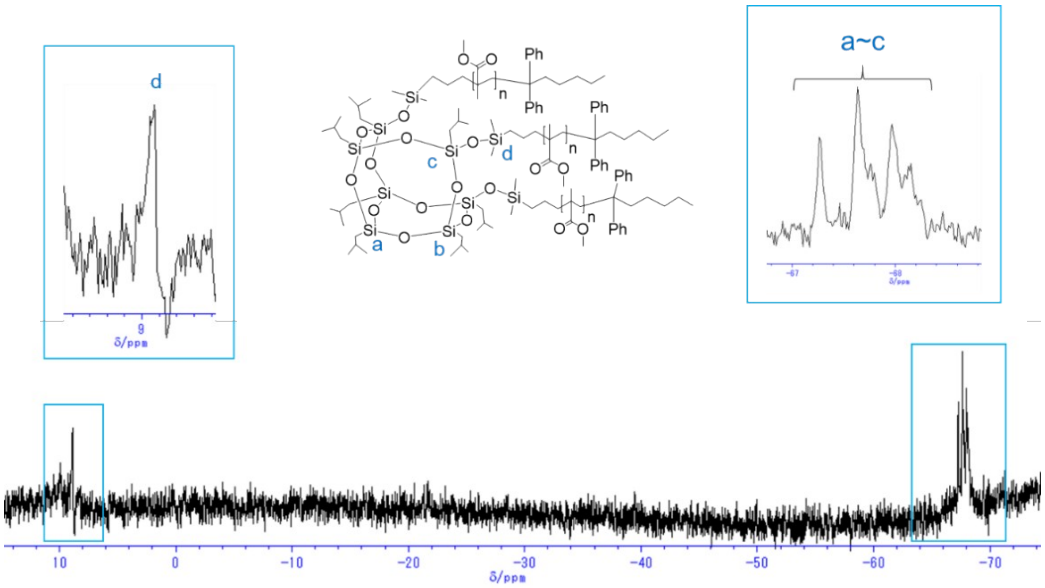


**Figure S9.** $^{29}$Si-NMR spectrum (80 MHz) of **3a** in $CDCl_3$.

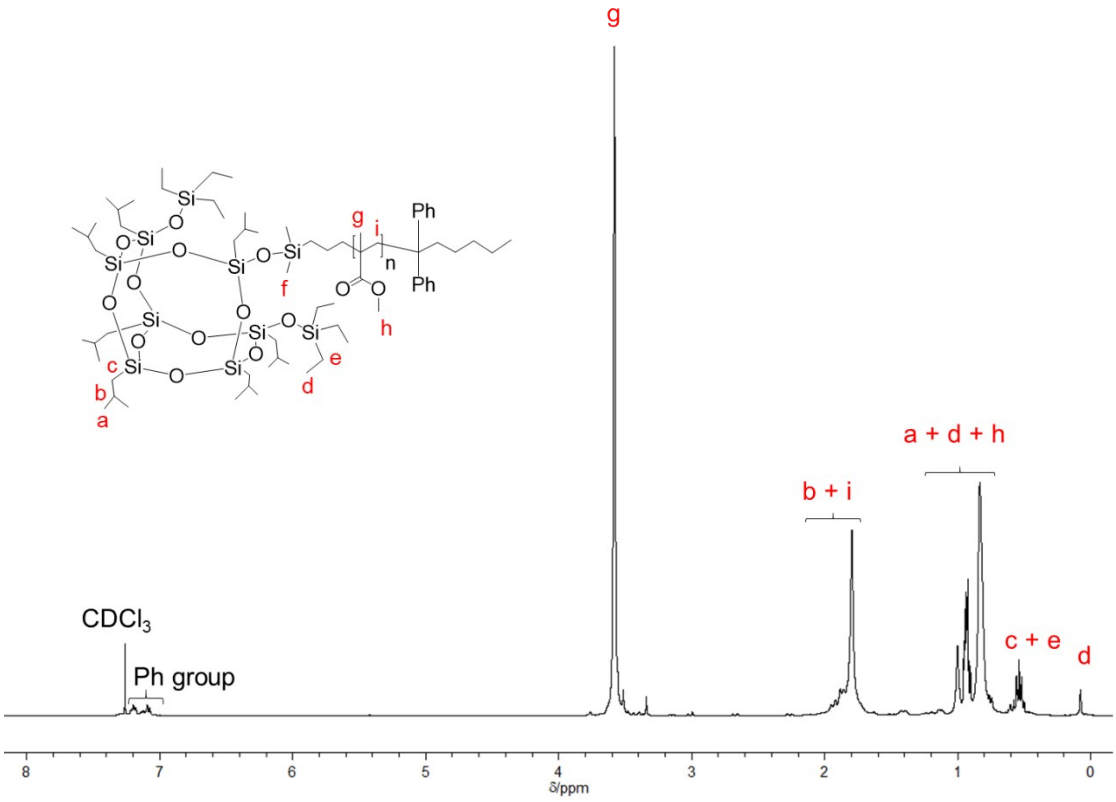


**Figure S10.** $^{1}$H-NMR spectrum (400 MHz) of **3b** in $CDCl_3$.

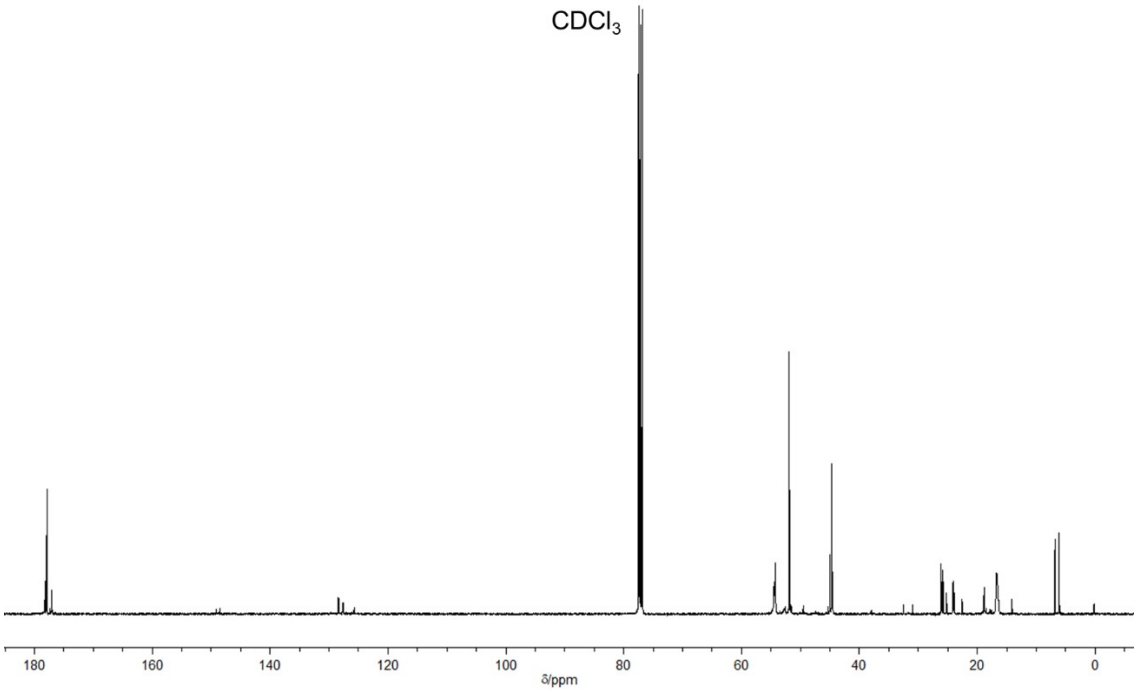


**Figure S11.** $^{13}$C-NMR spectrum (100 MHz) of **3b** in $CDCl_3$.

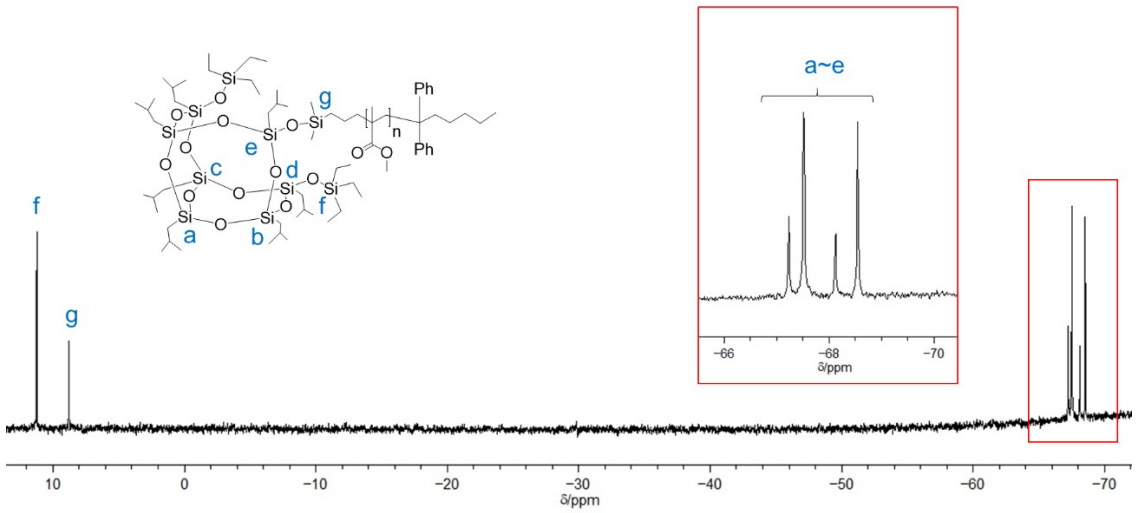


**Figure S12.** $^{29}$Si-NMR spectrum (80 MHz) of **3b** in $CDCl_3$.

## 2. MALDI-TOF MS spectra

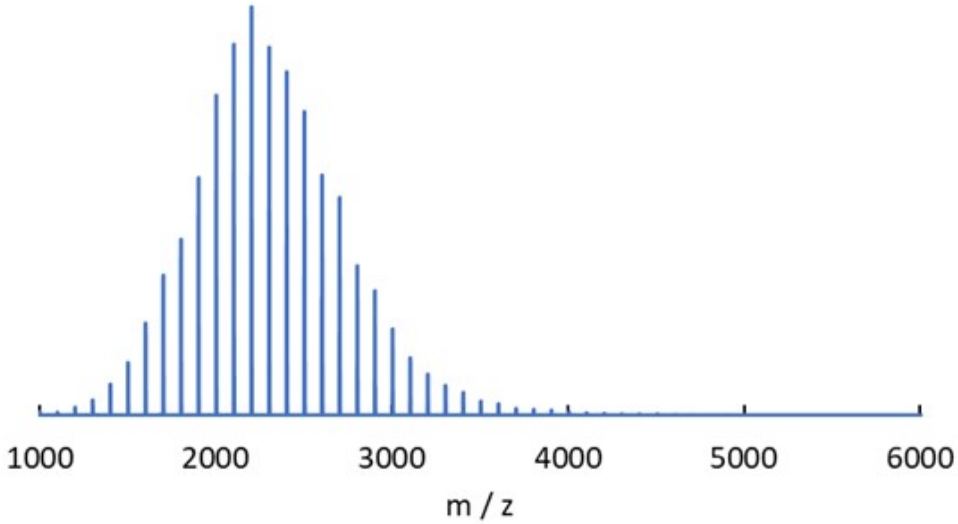


**Figure S13.** MALDI-TOF MS spectrum of **1a**.

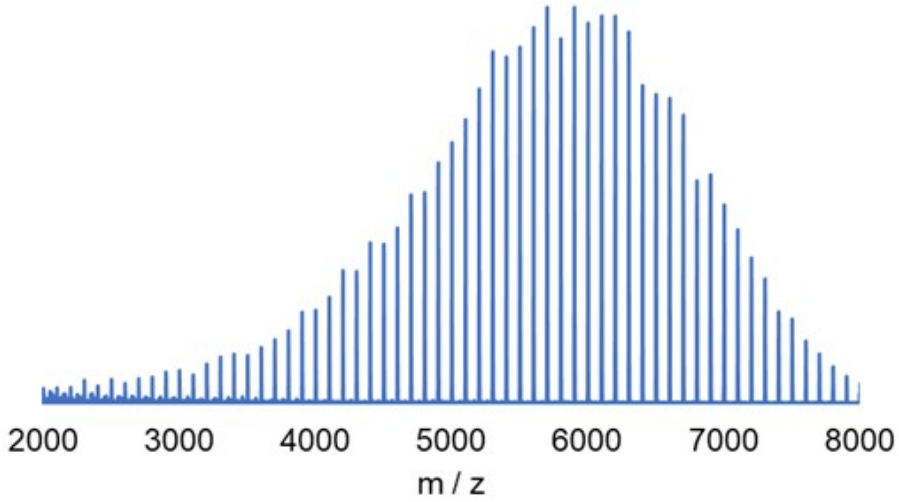


**Figure S14.** MALDI-TOF MS spectrum of **1b**.

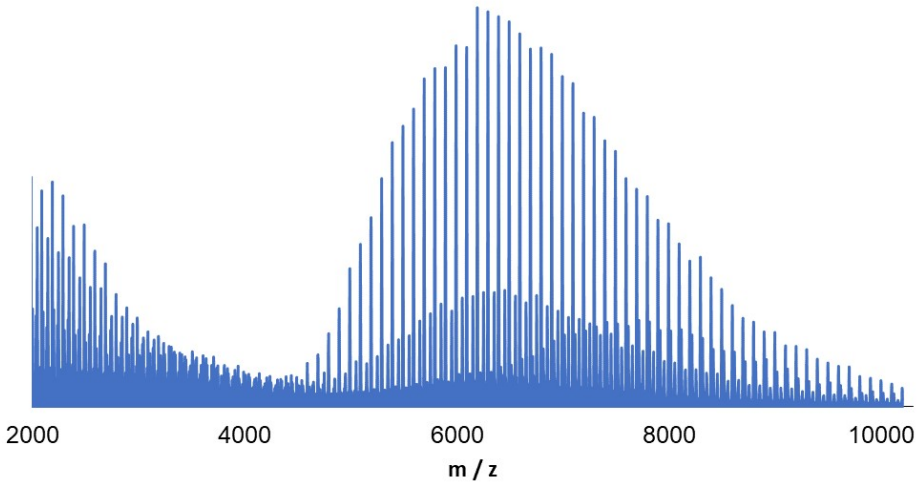


**Figure S15.** MALDI-TOF MS spectrum of **3a**.

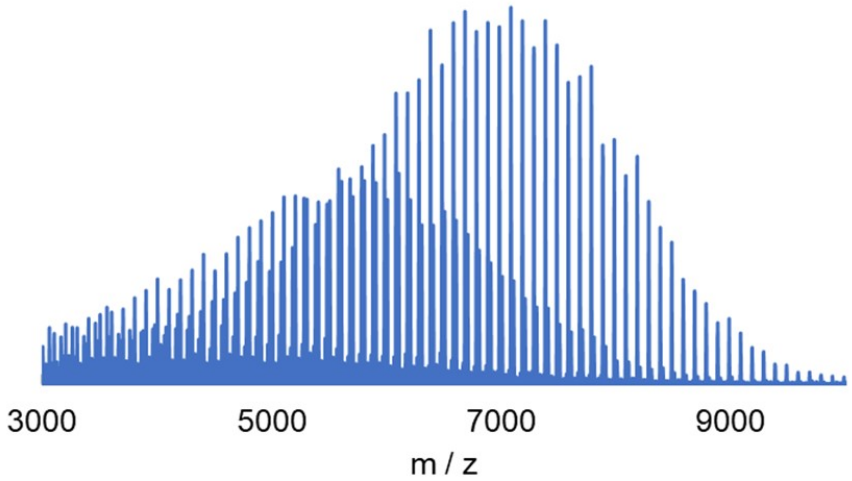


**Figure S16.** MALDI-TOF MS spectrum of **3b**.

## 3. SEC traces

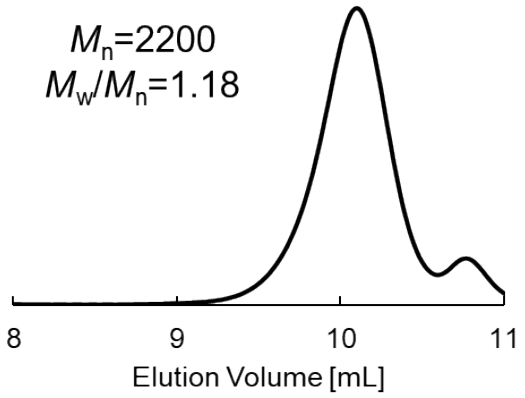


**Figure S17.** SEC trace of **1a** (1 ml/min in THF, RI detector).

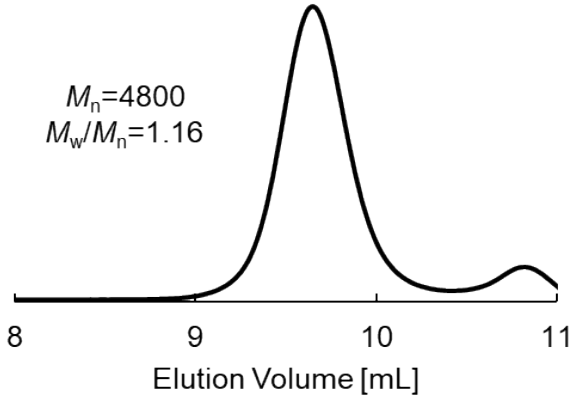


**Figure S18.** SEC trace of **1b** (1 ml/min in THF, RI detector).

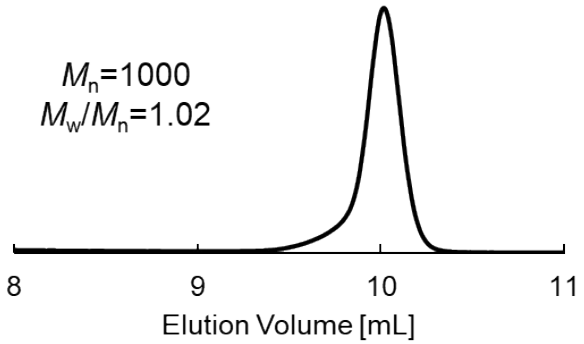


**Figure S19.** SEC trace of **2a** (1 ml/min in THF, RI detector).

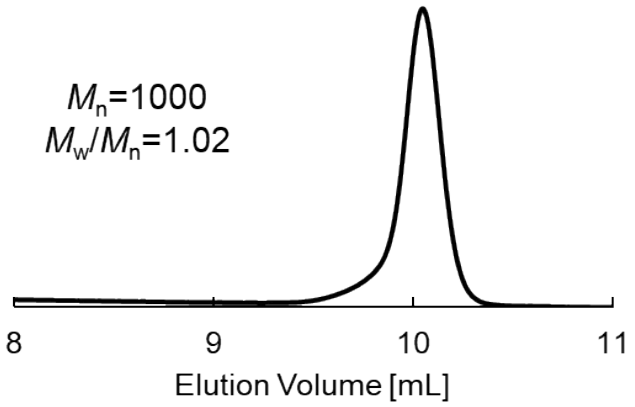


**Figure S20.** SEC trace of **2b** (1 ml/min in THF, RI detector).

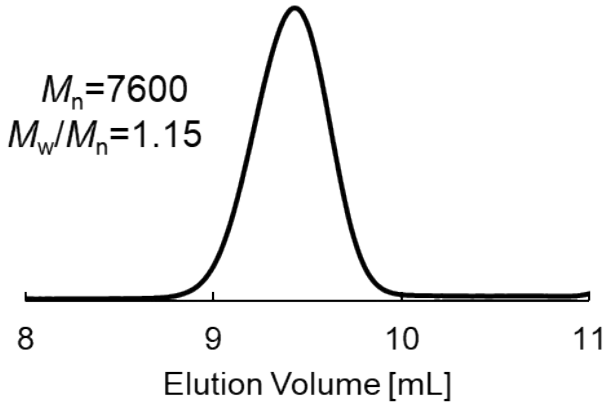


**Figure S21.** SEC trace of **3a** (1 ml/min in THF, RI detector).

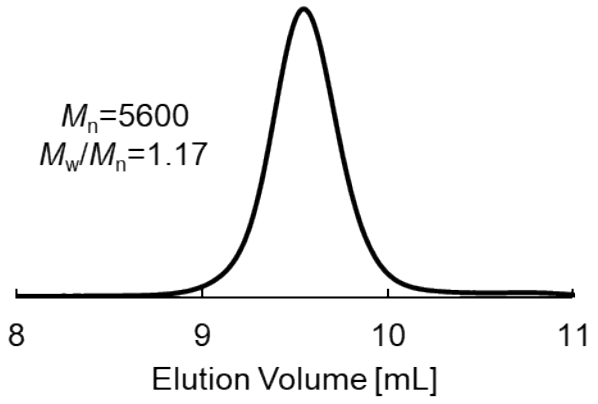


**Figure S22.** SEC trace of **3b** (1 ml/min in THF, RI detector).

## 4. SAXS analyses on the aggregation structures

In this section, we explain the details of the method how to estimate the distribution of the particle size for **3a** and **3b** (as-cast and annealed) based on the SAXS results. As mentioned in the main text, the SAXS profiles shown in Figure 7 exhibit the power-law behavior in the lower $q$ range with the shoulder or the peak around $q$ = 0.77 nm$^{-1}$. Assuming that the shoulder is ascribed to the particle scattering while the peak is due to the interference of the scattered X-ray due to the lattice ordering of the particles (so-called lattice factor), the following equation was used for the parameter fitting:

$$I(q) = k_1 q^{-n} + k_2 P(q) + k_3 L(q) \text{ --- (S1)}$$

The first term of the right-hand side expresses the power-law behavior, and the second and the third terms are the particle scattering $P(q)$ contribution and the lattice factor $L(q)$ as:

$$P(q) = \Sigma \{ n(R) (4\pi R^3/3)^2 [ F(q) ]^2 \} \text{--- (S2)}$$

$$L(q) = \exp [- (q - q^*)^2/(2\Delta q^2)] \text{ --- (S3)}$$

Here, $n(R)$ denotes the distribution function, and $F(q)$ is the structure amplitude as:

$$F(q) = 3/(qR)^3 [ \sin (qR) - qR\cos(qR)] \text{ --- (S4)}$$

Based on $n(R)$, the size distribution of the particles is estimated as:

$$\text{abundance (vol\%)} = n(R)R^3/ \Sigma \{n(R)R^3\} \times 100 \text{ --- (S5)}$$

Eq. (S3) is the Gaussian function which is used to express the peak empirically (not theoretically) peak with $q^*$ and $\Delta q$ being the peak position and determining the width of the peak, respectively.[1]

The value of $n$ in the first-term of the right-hand side of eq.(S1), $n$ = 3.5 was phenomenologically set for the annealed **3a** and the as-cast **3b**, while the Porod law with $n$ = 4 was considered for the as-cast **3a** and the annealed **3b** specimens. The prefactors of $k_1$, $k_2$ and $k_3$ are determined as parameters of the fitting, as well as $n(R)$, $q^*$ and $\Delta q$ as the fitting parameters. The parameter fitting (the least square fitting) has been conducted by using the software (Igor Pro® WaveMetrics). The results of the best-fit SAXS profiles are shown with red to the experimentally obtained SAXS profiles shown in black in Figure S23. For all of the specimens, the fitting worked very well, and the size distribution as shown in Figure 8 in the main text has been evaluated. Furthermore, the spacing of 7.24 nm and 6.56 nm from the position ($q^*$) of the lattice peak have been evaluated for the as-cast and the annealed **3b** specimens, respectively.

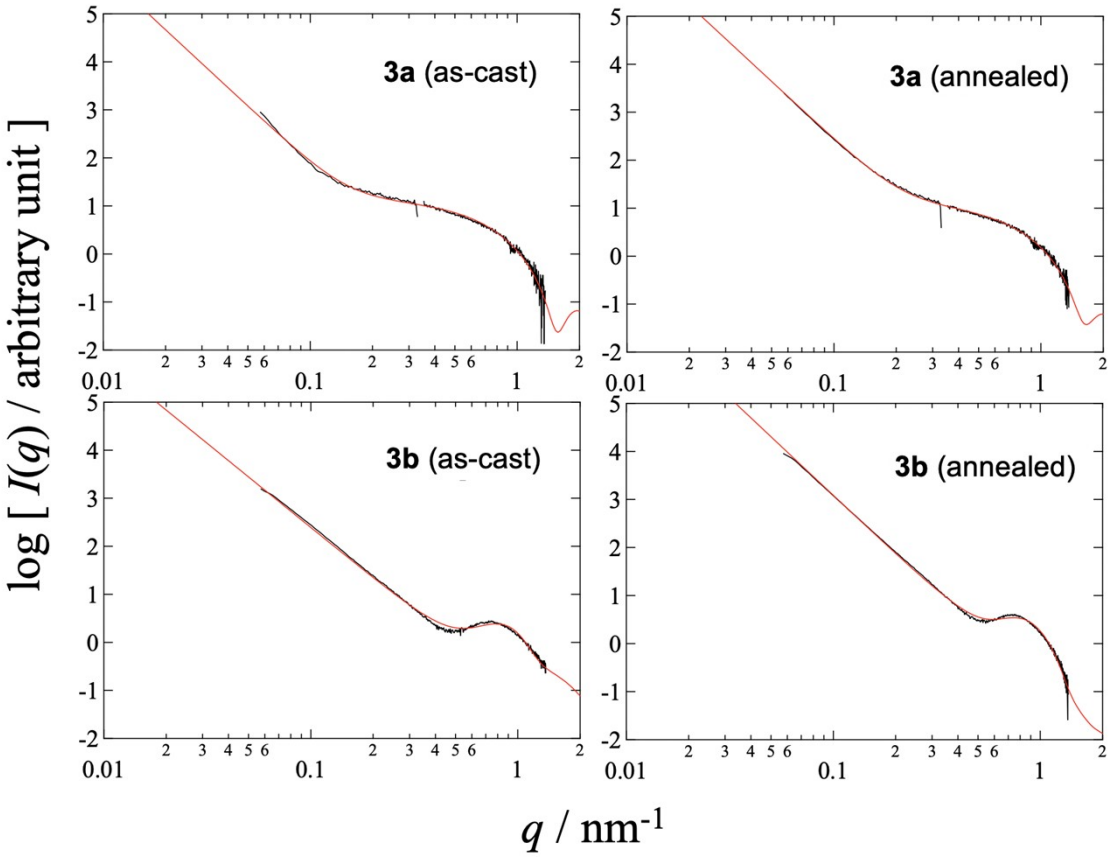


**Figure S23.** Comparison of the best-fit SAXS profiles (red) with the experimentally obtained SAXS profiles (black) for **3a** and **3b** (as-cast and annealed). The red curves are reproduced based on the parameters determined by the fitting.

Based on the most reliable size of the particles, which is 3 nm diameter for the as-cast **3b** specimen, the thickness of the PMMA shell is estimated in the main text by assuming the closest contact of the two-neighboring particles, as shown in Figure S24. For this specimen, the distance between the center of gravity of the two-neighboring particles was also determined as 7.24 nm from the $q^*$ value through the relationship of $d = 2\pi/q^*$. In this illustration, there seems to be an open space in the middle of the center of gravity of three particles. However, this illustration is just simplified for the sake of the brief explanation of the core-shell structure and it is noted that such the open space should be filled with unimers (which are the molecules without forming any aggregations).

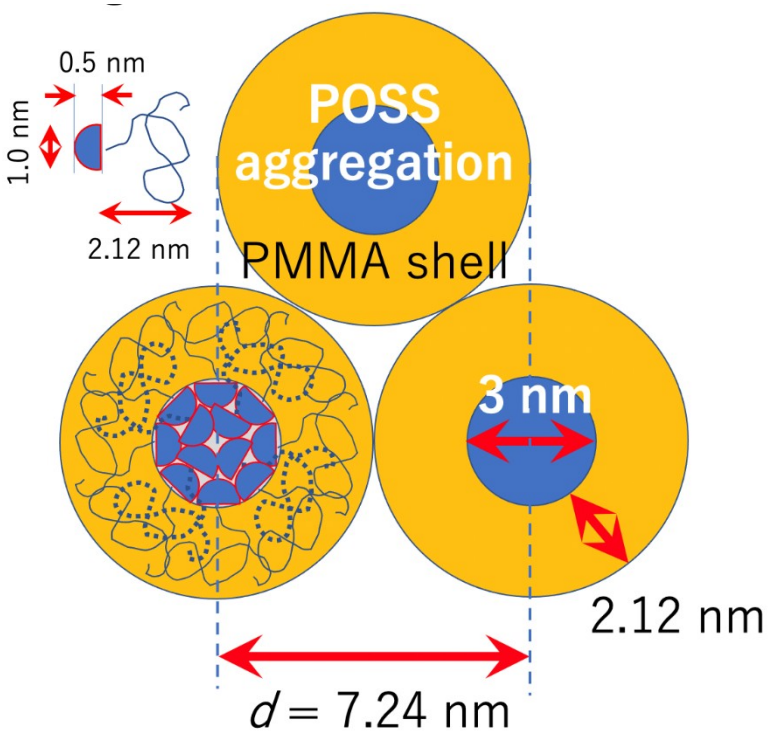


**Figure S24.** Schematic illustration for the core-shell model of the aggregated particles of the corner-opened POSS with the PMMA chains for the as-cast **3b** specimen. Note that the 3 nm diameter and the *d* value were determined through the parameter fitting of the SAXS profile. The core (blue) and the shell (orange) are composed of the aggregated CO-POSS moiety and the PMMA chains, respectively. Based on this closest contact of the particles, the thickness of the PMMA shell is so determined as 2.12 nm. This value is less than the molecular dimension of the PMMA moiety of **3b** specimen (3.78 nm) being evaluated by assuming a random coil of the Gaussian chain. Coupled with the half-dimension of POSS with 1-nm diameter, molecular packing in an aggregated particle is schematically shown together. The blue broken curve stands for the PMMA chain being attached to the CO-POSS moiety located in the interior of the core (far from the interface to the PMMA shell), while the blue solid curve dose for the PMMA chain being attached to the corner-opened POSS moiety located near the interface. For detailed discussion, see below.

## 5. More detailed discussion on the aggregated particles

In Figure 7 in the main text, the SAXS profiles for **1a** and **1b** clearly indicate a power-law behavior as $I(q) \sim q^{-4}$, which is well known as the Porod law. Since this law indicates smooth surface of particles, the existence of such particles in the glassy PMMA homopolymer may suggest inhomogeneous structure (nodule structure in glassy polymers) or frozen density fluctuation in the glassy structure.[2]

On the contrary, the SAXS profiles for **3a** and **3b** exhibit a shoulder and a peak around $q$ = 0.77 $nm^{-1}$, respectively, while the scattering intensity follows the power-law behavior in the lower $q$ region with the exponent of -4 (excepting for the annealed **3a** and the as-cast **3b** which show the lower exponent value of -3.5). This power-law behavior is the same as that observed for **1a** and **1b** as the glassy PMMA homopolymer.

The as-cast **3a** specimen exhibits the mono-disperse feature with the diameter of 6 nm, which is twice larger as compared to that for the as-cast **3b**. The flexibility of the PMMA chains is considered to be larger for **3b**. This feature may increase significance of the contribution from the conformational entropy to the total free energy, as compared to the case of **3a** where the 1/3 molecular weight of the PMMA chains can be more or less stretched in the radial direction of the core-shell particles (a similar structure of a crew-cut micelle) without significant loss of the conformational entropy. Thus, the size of the particle can be larger than that for **3b**.

Here, it is worth to estimate quantitatively the chain dimensions of PMMA for the **3a** and **3b** specimens. To estimate the values of $n$ in Scheme 1, the contribution of the end groups (allyl group, *n*-BuLi and DPE) was eliminated. Thus, $n$ = 23.2 and 52.9 as weight-averaged values were obtained for the case of the **3a** and **3b** specimens, respectively. For the case of the fully extended conformation, we assume the 10/1 helical conformation with 2.08-nm of the period for isotactic PMMA.[3] Thus, the lengths of the fully extended PMMA chains were evaluated to be 4.82 and 11.0 nm for the case of the **3a** and **3b** specimens, respectively. On the contrary, the radius of gyration for the unperturbed chain dimension was estimated to be 1.25 and 1.89 nm for the case of the **3a** and **3b** specimens, respectively, according to the data obtained for the dilute solution of the isotactic PMMA in the theta state.[4]

As schematically illustrated in Fig. S24, the thickness of the PMMA (2.12 nm) is much lesser than the length of the fully extended chain (11.0 nm) so that the PMMA chains prefer the random-coil conformation due to the entropy gain for a comparatively larger value of the degree of polymerization ($n$) of the PMMA moiety for the **3b** specimen. Nevertheless, the thickness value of the PMMA shell (2.12 nm) is even less than the molecular dimension of the PMMA moiety of **3b** specimen (3.78 nm; twice of the radius of gyration value of 1.89 nm). This fact suggests compression of the PMMA chain conformation, which may be due to the solvent evaporation. Due to such compression, the aggregation particles with smaller size may receive frustration. As a matter of fact, larger particles were formed after the thermal annealing,

as shown in Fig. 8, which is expected to be triggered by the relaxation of the compressed PMMA chains.

Calculated from the density value of PMMA (1.18 g/cm$^3$), it was estimated that 23.4 molecules of **3b** were involved in the aggregation particle. Coupled with the half-dimension of POSS with 1-nm diameter, molecular packing in an aggregated particle is schematically shown together in Fig. S24. The blue broken curve stands for the PMMA chain being attached to the CO-POSS moiety located in the interior of the core (far from the interface to the PMMA shell), while the blue solid curve dose for the PMMA chain being attached to the corner-opened POSS moiety located near the interface. Although the part of the PMMA chain solubilized in the CO-POSS core (illustrated with the blue broken curve) should receive tremendous frustration from the CO-POSS moieties due to the exclusive (repulsive) segregation effects, the length of such part is at most 0.5 to 1.0 nm, as illustrated in Fig. S24. Again, this situation may result in the tremendous change in the particle size distribution after the thermal annealing, as shown in Fig. 8. Since we have estimated that 23.4 molecules of **3b** were involved in the CO-POSS core, the density can be evaluated. By neglecting the contribution of the partial PMMA solubilization in the core, it was estimated to be 1.17 g/cm$^3$. This value seems to be reasonable by consideration from the chemical structure of CO-POSS.

Finally, we try to illustrate a similar aggregation structure for the as-cast **3a** specimen. First of all, the diameter of the CO-POSS core is 6 nm (according to the result shown in Fig. 8). Then, from the density value of CO-POSS (afore-mentioned to be 1.17 g/cm$^3$), the number of molecules involved was so estimated to be 187. Finally, the thickness of the PMMA shell for the **3a** specimen was estimated to be 5.0 nm. This value is very close to the length of the fully extended PMMA chains (4.82 nm) with $n$ = 23.2 for the **3a** specimen. Therefore, it can be concluded that the PMMA chains of the **3a** specimen is fully extended due to the small value of the degree of polymerization (less importance of the entropic contribution to the chain dimension). Nevertheless, the molecular packing illustration was failed because of the too-large diameter of the CO-POSS core in which 187 CO-POSS moieties were estimated to be involved. The fully extended PMMA chains attached to the CO-POSS core located near the center of the core (far from the interface) should be mixed with POSS at least in the length of 2 nm, which is almost 42% of the length of the fully-extended PMMA chain. This situation is too unrealistic and the drawing of the molecular packing illustration in the aggregation particle for the **3a** specimen is nightmare.

**References**


[1] "Nanomorphology Characterization of Sterically Stabilized Polypyrrole-Palladium Nanocomposite Particles", H. Takeoka, N. Fukui, S. Sakurai, Y. Nakamura, S. Fujii, *Polym. J.* **2014**, *46*, 704-709.

[2] “On the structure of glassy polymers. II. Small-angle x-ray scattering from poly(methyl methacrylate)”, A. L. Renninger, D. R. Uhlmann, *J. Polym. Sci., Part B, Polym. Phys. Ed.* **1975**, *13*, 1481-1490.

[3] H. Kusanagi, *Kobunshi Ronbunshu* **1996**, *53*, 415-422.

[4] T. Yoshizaki, *Kobunshi* **2007**, *56*, 416-419.